

Altermagnetism from interaction-driven itinerant magnetism

Samuele Giuli,^{1,*} Carlos Mejuto-Zaera,¹ and Massimo Capone^{1,2}

¹*International School for Advanced Studies (SISSA), via Bonomea 265, 34136 Trieste, Italy*

²*CNR-IOM Democritos, Via Bonomea 265, 34136 Trieste, Italy*

(Dated: October 2, 2024)

Altermagnetism, a new phase of collinear spin-order sharing similarities with antiferromagnets and ferromagnets, has introduced a new guiding principle for spintronic/thermoelectric applications due to its direction-dependent magnetic properties. Fulfilling the promise to exploit altermagnetism for device design depends on identifying materials with tuneable transport properties. The search for intrinsic altermagnets has so far focused on the role of anisotropy in the crystallographic symmetries and in the bandstructure. Here, we present a different mechanism that approaches this goal by leveraging the interplay between a Hubbard local repulsion and the itinerant magnetism given by the presence of van Hove singularities. We show that altermagnetism is stable for a broad range of interactions and dopings and we focus on tunability of the spin-charge conversion ratio.

Introduction. The landscape of magnetic systems has been thrilled by the proposal and experimental realization of altermagnetism, a new type of collinear spin-order which shares similarities with both antiferromagnets and ferromagnets [1, 2], while featuring new properties that hold a huge potential for fundamental science and applications. Altermagnets are characterized by a zero net magnetization in the non-relativistic limit, similarly to antiferromagnets, but their electronic bands do not form a Kramer doublet, having instead a momentum-dependent spin-splitting. Importantly, the magnetic polarization of an altermagnet has a long-range order with d-wave (or higher, g- or i-wave) symmetry characterized by nodes. The applicative potential of altermagnets relies mostly on the anisotropic magnetic properties which have been proposed to give rise to giant magnetoresistance (GMR) [1], giant tunnel magnetoresistance [3], non-vanishing spin splitting torque [4, 5] as well as anomalous Hall conductivity [6, 7].

Despite the impressive and rapidly increasing body of work introducing candidate materials for altermagnetic ordering [8? ? –20], there are still few experimental evidences of this phase of matter. This is in part due to the lack of spin-resolved measurements and the small non-relativistic spin-splitting, which poses a challenge to its experimental resolution. For RuO₂ films various altermagnetic phases have been realised [21] while the debate for bulk RuO₂ [22, 23] is still open. Compelling evidence for altermagnetic ordering has been presented instead for MnTe [24] and CrSb [25]. Recently, it has been proposed that this direction-dependent magnetic phase could also arise from anisotropic local orbital states [26] where inter-

actions can trigger the presence of an altermagnetic phase with the simultaneous realisation of orbital and magnetic ordering.

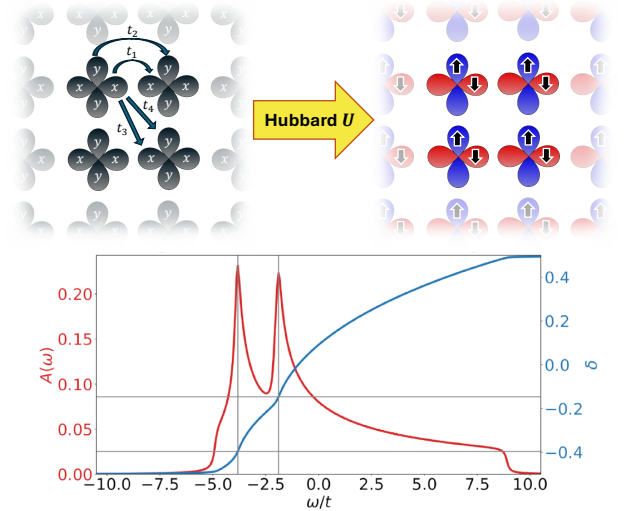


Figure 1: Illustration of the interaction-driven phase transition from paramagnetic (top left) to altermagnetic (top right) and density of state of the non-interacting model (bottom-left axis) with doping (bottom-right axis) of the van Hove singularities in the non-interacting limit.

In the search for intrinsic altermagnetic materials, most proposals have leveraged chemical and structural manipulation to tailor the electronic structure. Yet, recently an alternative approach to let altermagnetism arise from interactions has gained traction [10, 18, 26]. This direction offers a particularly attractive perspective: devising platforms with *tunable* altermagnetic properties exploiting strong electronic correlations, which characterizes ma-

* Correspondence email address: sgiuli@sissa.it

terials with narrow bands and comparatively large values of the screened Coulomb repulsion.

Indeed, the two traditional collinear magnetic phases, ferromagnetism and antiferromagnetism, are linked to strong correlation physics. Antiferromagnetism is an ubiquitous signature of strong correlations in undoped materials, while itinerant ferromagnetism is naturally connected with doped correlated materials.

The presence of ferromagnetism in the Hubbard model has been one of the driving forces behind the very introduction of the model. According to Nagaoka's theorem, it is the groundstate for a single hole and large interactions [27], and it has been found in finite interactions [28–31] and for frustrated systems [32, 33] as well. In the triangular lattice Hubbard model the presence of a Van Hove singularity (vHs) at filling $n = 3/4$ appears to be fundamental for the formation of itinerant ferromagnetism [34] and also in the $t - t'$ square lattice Hubbard model [29, 35]. In twisted bilayer graphene, the presence of a vHs near half-filling has also been linked to s -wave and $s\pm$ -wave Pomeranchuk instabilities [36, 37]

In this work, building on the above arguments, we propose a new paradigm where electronic correlations lead to the onset of altermagnetic ordering. Our proposal is based on a two-orbital model with anisotropic orbitals, and a van Hove singularity at moderate doping (See Figure 1). We show that the altermagnetic ordering naturally emerges as a result of the cooperation between the correlation-driven itinerant magnetism and the C_{4z} symmetry of inequivalent orbitals with a uniform, on-site, non-relativistic spin-splitting. This mechanism relies on intrinsic correlation effects due to a local Hubbard repulsion that is not devised to explicitly break the spin and orbital symmetries. For this reason it can be realized in generic lattices even when spatial ordering is frustrated. These features are indeed quite generic and could inspire the ab-initio and experimental search for altermagnetism candidates in unexplored classes of materials.

Model. We focus on a model introduced soon after the discovery of superconductivity in iron-based materials [30] as a minimal theoretical description. This model features two degenerate orbitals of d_{xz} and d_{yz} symmetry on each lattice site and local interactions parameterized by the intraorbital Hubbard U . The one-body Hamiltonian on a square lattice reads:

$$\hat{H}_0 = \sum_{\mathbf{k}, s} \begin{pmatrix} c_{\mathbf{k}xs}^\dagger & c_{\mathbf{k}ys}^\dagger \end{pmatrix} \begin{pmatrix} \epsilon_x(\mathbf{k}) & \epsilon_{xy}(\mathbf{k}) \\ \epsilon_{xy}(\mathbf{k}) & \epsilon_y(\mathbf{k}) \end{pmatrix} \begin{pmatrix} c_{\mathbf{k}xs} \\ c_{\mathbf{k}ys} \end{pmatrix} \quad (1)$$

with

$$\begin{aligned} \epsilon_x(\mathbf{k}) &= -2t_1 \cos k_x - 2t_2 \cos k_y - 4t_3 \cos k_x \cos k_y \\ \epsilon_y(\mathbf{k}) &= -2t_2 \cos k_x - 2t_1 \cos k_y - 4t_3 \cos k_x \cos k_y \\ \epsilon_{xy}(\mathbf{k}) &= -4t_4 \sin k_x \sin k_y \end{aligned} \quad (2)$$

We set $t_1 = -t$, $t_2 = -1.75t$, $t_3 = -0.85t$, and $t_4 = -0.65t$, following Ref [26]. This choice of parameters results in two van Hove singularities (vHs) in the bare density of states at doping $\delta_{vH} \approx -0.145$ and $\delta_{vH,2} \approx -0.396$. The existence of these vHs, together with the structure of the hoppings reflecting the d_{xz} and d_{yz} character of the orbitals, turn out to be the key ingredient to drive the altermagnetic state. Therefore, our results do not rely in the specific values of parameters as long as a vHs at reasonably small doping is present.

We will indeed focus on the doping region around the first vHs since the effect of the interaction around the second singularity is strongly reduced by the extreme doping. We introduce a purely intra-orbital Hubbard interaction, which, as discussed above, favours a ferromagnetic state close to a vHs on the single band Hubbard model [27–29]. The local interaction Hamiltonian therefore reads:

$$\hat{H}_{int} = U \sum_{i, \alpha=x, y} (n_{i\alpha\uparrow} - \frac{1}{2})(n_{i\alpha\downarrow} - \frac{1}{2}) \quad (3)$$

where $n_{i\alpha s}$ is the density operator at site i , orbital α and spin s .

Method. We solve this model using the ghost rotationally invariant slave boson (gRISB) approach with mean-field boson decoupling [38], which is a generalization of RISB [39, 40] and equivalent to the ghost Gutzwiller method [41]. This is a non-perturbative, variational Ansatz to capture strong electronic correlation in model as well as *ab initio* calculations of solids and molecules [38, 41–49]. Within its embedding formulation, gRISB represents an interacting systems in terms of a pair of quasiparticle (qp) and impurity Hamiltonians. The latter captures local correlations exactly, while the former features interaction-renormalized hoppings and one-body potentials. The parameters of these Hamiltonians are determined self-consistently by matching their local one-body density matrices $\langle c_\alpha^\dagger c_\beta \rangle$, which makes the method computationally inexpensive [48, 50, 51]. Thus, we can use gRISB to rapidly and thoroughly explore the phase diagram of the multi-orbital model in Eq. (1)-(3), obtaining faithful local order parameters from the impurity Hamiltonians, as well as non-local correlation functions from the band structure of the qp Hamiltonian. The description of correlated behavior in terms of a band structure theory greatly simplifies the study of the altermagnetic phase

and its properties, and is enabled by the introduction of auxiliary states in the qp Hamiltonian, the eponymous ghosts. These ghosts enable capturing incoherent high-energy spectral features, for instance Hubbard bands, on top of the low-energy quasiparticle excitations [41, 44, 48]. Throughout the paper we fix the number of ghost orbitals per physical band to be $N_{ghosts} = 2$. The main equations of the gRISB formalism are summarized in the Supplementary Material (SM) [52].

Results. We define the local altermagnetic order parameter as

$$\Delta_{alm} = \frac{m_x - m_y}{2} \quad (4)$$

with $m_\alpha = n_{\alpha\uparrow} - n_{\alpha\downarrow}$ the spin magnetisation on orbital $\alpha = x, y$. We present the ground state phase diagram in Figure 2. The presence of the vHs at doping $\delta_{vH} \approx -0.145$ (shown as a vertical, dashed line in Fig. 2) is linked to the onset of spin ordering at large interaction U with two orbitals having opposite magnetisation, realising the altermagnetic phase we propose in this paper. In contrast to previously proposed interaction-driven altermagnetic phases [26], we note that the opposite magnetic moments related by C_{4z} symmetry reside on *the same atomic site*. The altermagnetic ordering is enhanced and it extends to a larger range of dopings with increasing U/t while the maximum of the order parameter at fixed interaction is always found near $\delta = \delta_{vH}$. Significant interactions result therefore in a large doping region where altermagnetism is stable and sizeable, avoiding the need for fine tuning the chemical potential, a particularly important point in view of applications to materials. The altermagnetic phase is also characterized by the momentum-dependent Zeeman splitting shown in the gRISB bandstructure on the right side of Fig. 3(a).

Our proposed altermagnetic state is energetically favorable with respect to a fully ferromagnetic one due to the presence of inter-orbital hoppings that, together with the local repulsion U , favor antialignment of the spins between the orbitals (see SM [52]). In addition, the presence of large next-nearest-neighbor hoppings (t_3 and t_4 in Eq. (2)) frustrates bipartite ordering, therefore we expect the altermagnet to be stable with respect to other uniform or non-uniform orderings. Further including inter-orbital interaction terms, that we neglected for the sake of simplicity, are not expected to destroy the altermagnetism as long the intra-orbital U remains the largest energy scale, a condition which holds under very general circumstances.

As we mentioned above, transport properties are amongst the most appealing features of altermagnets. For instance, these phases allow for spin-splitter effect when applying an electric field in the [110] direction. Since

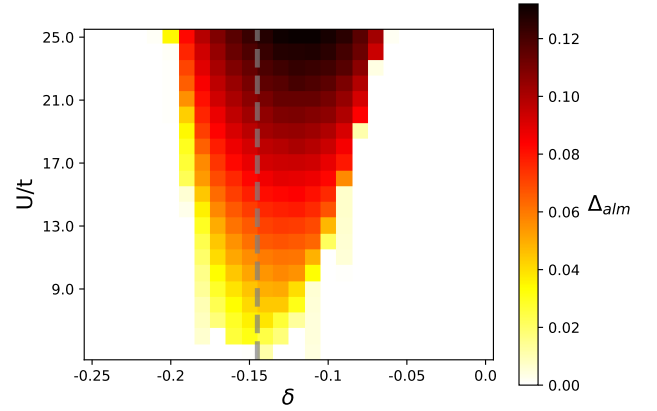


Figure 2: Altermagnetic order parameter Δ_{alm} in Eq. (4) as a function of the interaction U and doping δ . The gray dashed vertical line indicates the doping of the van Hove singularity in the non-interacting model.

\hat{S}_z remains a good quantum number, we can compute the spin-independent conductivity for spin-up and spin-down:

$$\sigma_{ab}^s(\omega) = -e^2 \frac{\langle \frac{1}{V_{BZ}} \sum_{\mathbf{k}} \partial_{k_a} \partial_{k_b} H_{\mathbf{k}}^s \rangle - \Lambda_{ab}^s(\omega)}{i(\omega + i0^+)} \quad (5)$$

with $s = \uparrow, \downarrow$, where $\Lambda_{ab}^s(\omega)$ is the s -spin current-current dynamical response that we compute as the elementary bubble without vertex corrections [53, 54].

In the case of a static electric field in the [110] direction the spin current \mathbf{j}_s is orthogonal to the charge current \mathbf{j}_c [5, 26], hence we can use the Drude weight defined as

$$D_{ab}^s = \langle \frac{1}{V_{BZ}} \sum_{\mathbf{k}} \partial_{k_a} \partial_{k_b} H_{\mathbf{k}}^s \rangle - \Lambda_{ab}^s(\omega = 0) \quad (6)$$

to compute the charge-spin conversion ratio R as

$$R = \frac{|\mathbf{j}_s|}{|\mathbf{j}_c|} = \frac{\sqrt{\sum_a (j_a^\uparrow - j_a^\downarrow)^2}}{\sqrt{\sum_a (j_a^\uparrow + j_a^\downarrow)^2}} \quad (7)$$

where $j_a^s = \sum_\beta D_{ab}^s A_b$ and $A_b = A$ is the vector potential for $a, b = x, y$ directions.

We plot the ratio R in Figure 3 (b) with a positive sign for spin current in the [-110] direction and negative for the opposite one. We notice an enhancement of R when increasing both doping and/or the interaction U/t . The ratio rises up to $R \approx 9\%$ for a typical value of $U/t =$

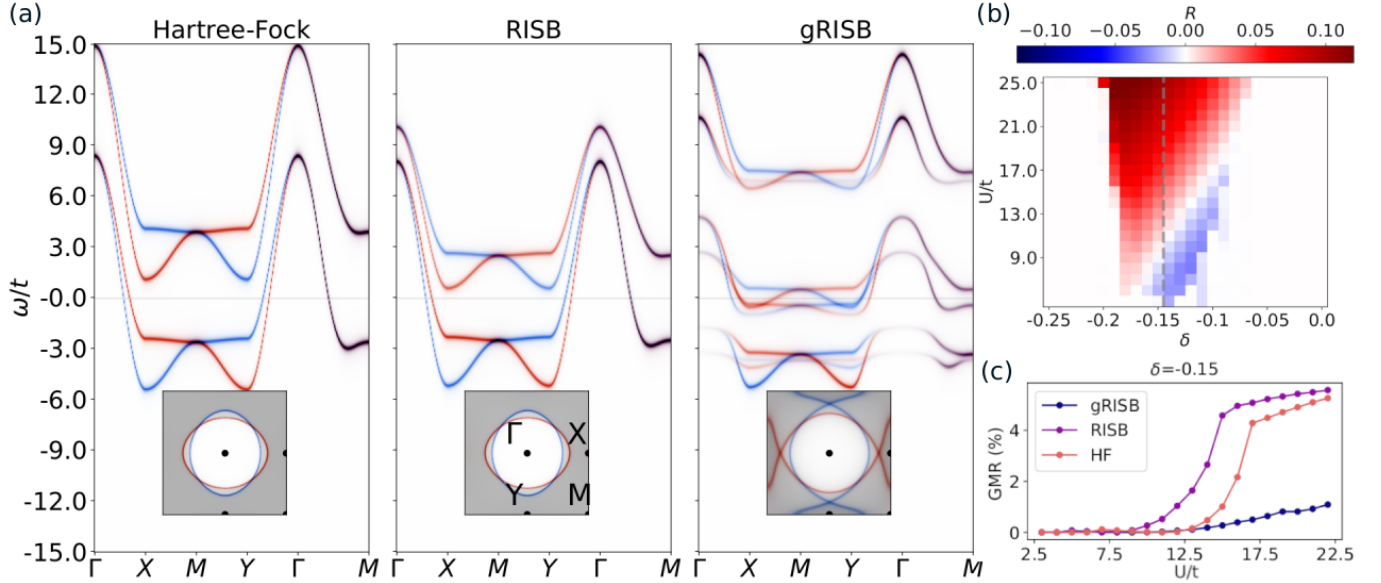


Figure 3: (a) Spin up (red) and spin down (blue) spectral functions along symmetry lines for $U/t = 20$ and $\delta = -0.15$ using Hartree-Fock (left), RISB (center) and gRISB (right) with 2 ghosts. In the insets, the respective Fermi surfaces along the Brillouin zone, the shadowed area represent fermionic occupation: dark occupied, light empty. (b) Charge spin conversion ratio in Eq. (7) as a function of interaction (U/t) and doping (δ). Positive values correspond to spin-current in the $[-110]$ direction while a negative ones are in the opposite direction. The gray dashed vertical line indicates the doping of the van Hove singularity in the non-interacting model. (c) GMR comparison between gRISB(dark), RISB(medium) and HF(light).

20, corresponding to an angle between the spin-up and spin-down currents of $\theta \approx 10^\circ$. We also notice that the spin current changes sign along a straight line in our U - δ diagram.

The inversion of the spin current is related to the different spin polarization of the carriers in x and y orbitals. The Drude weight is dominated by the contribution of the electrons at X in the Brillouin zone (See SM [52]). The X orbital hosts a majority of spin-up carriers while the Y orbital a majority of spin-down carriers. This phenomenon opens the possibility of changing the sign of the spin current tuning the interaction via mechanical or chemical pressure.

In order to assess how relevant strong correlations are to this altermagnetic ordering, we plot the band structure for an interaction $U/t = 20$ and doping $\delta = -0.15$ for Hartree-Fock (HF, left), RISB (center) and gRISB (right) in Figure 3 (a). The HF and RISB result are qualitatively similar, with the latter showing a moderate renormalisation due to the local Hubbard interaction. The gRISB band structure instead shows a stronger renormalisation and a large transfer of spectral weight toward the lower and

upper Hubbard bands. Moreover, the effect of strong correlation clearly reduces the non-relativistic spin-splitting and, more importantly, also changes the topology of the Fermi surface as shown in the insets of Figure 3 (a) with only gRISB predicting the presence of pockets around X and Y points in the Brillouin zone at large U/t . The presence of Dirac band crossing along the ΓX , ΓY , MX and MY lines is present only in the gRISB calculations for strong interactions. The reason is the existence of the following critical condition on the intra-orbital magnetic gap (Δ_{mag}) above which the Dirac points disappear (See SM and [18]).

$$\frac{\Delta_{mag}}{|t_1 - t_2|} \leq 1 \quad (8)$$

The reduction of the magnetic gap in gRISB is a key ingredient for the persistence of Dirac points. As shown in pannel (c) of Figure 3, the giant magnetoresistance, defined as:

$$GMR = \frac{1}{2} \left(\frac{\sigma_{xx}^\uparrow}{\sigma_{xx}^\downarrow} + \frac{\sigma_{xx}^\downarrow}{\sigma_{xx}^\uparrow} - 2 \right) \quad (9)$$

is also dramatically reduced by the inclusion of the high-energy ghosts improving the description of dynamical correlation effects. We observe indeed a reduction of a factor of almost 5 when comparing gRISB to RISB in the large interaction limit. This effect could partially resolve the mismatch between density functional theory predictions of ALM and the lack of spin-gap resolution in ARPES experiments.

Conclusions and Outlook. We proposed a new microscopic mechanism for interaction-generated altermagnetism linked to itinerant magnetism in the vicinity of a simple van Hove singularity, and we reported numerical evidence for its realization in a two-orbital model whose non-interacting bandstructure was introduced to describe iron-based superconductors. The altermagnetic state appears in a wide range of dopings and values of the interaction strength, presenting a maximum of the order parameter centered near the van Hove singularity δ_{vH} .

We analyzed the charge-spin conversion ratio responsible for the spin-splitter effect of the altermagnetic state and we observed a change of the spin current direction as a function of doping and interaction. This phenomenon opens the intriguing possibility to control the direction of the spin-current tuning the interaction exerting mechanical or chemical pressure on candidate materials.

Finally we discussed the effect of strong correlations beyond mean-field in the theoretical description. These clearly affect the nature of the altermagnetic state changing the shape of the band structure and the topology of the Fermi surface. As a result, they reduce the altermagnetic spin gap and giant magnetoresistance with respect to simple mean-field calculations (Hartree-Fock). This effect could justify the difficulties to experimentally find photo-emission evidence for altermagnetism in strongly correlated compounds. We note that a related mechanism has been proposed for κ -Cl in Ref. [19] which, unlike here, requires two coincident van Hove singularities at the M point to stabilize altermagnetic ordering.

Possible realisations of this mechanism could be found in Fe-based materials where evidence for altermagnetism has been reported for Hematite ($\alpha - \text{Fe}_2\text{O}_3$) [17] and FeSe [16]. Further, systems where the t2g orbital physics is dominant, like Ca_2RuO_4 [8], could be suitable plat-

form when the t2g bands are partially filled. Another promising platform are Moiré systems, where electronic properties can be tailored precisely and a wide palette of systems can be designed. In this context, evidence of itinerant ferromagnetism linked to the presence of a van Hove singularity [55–57] and numerical evidence of altermagnetic ordering [58, 59] have been reported.

In general, we emphasize the three key ingredients of our mechanism: (i) Two anisotropic orbitals related by a proper or improper rotation (e.g. in the model we present the x and y orbitals are related by C_{4z} symmetry) (ii) a strong local Hubbard interaction U and hoppings between the two orbitals to generate direct inter-orbital spin exchange and (iii) the presence of a vHs at an incommensurate filling promoting itinerant magnetic properties.

Moreover, frustration due to the lattice (e.g. triangular lattice) or due to hopping terms beyond nearest-neighbours (e.g. t_3 in this paper) opposes to bipartite ordering, hence favoring our altermagnetic state. In addition, materials with the previous properties and an inverted Hund’s coupling J arising from electron-lattice coupling [60, 61] may have an increased tendency to anti-align the spins on different orbitals, assisting the altermagnetic ordering we presented. Conversely, a positive sign J would only favor inter-orbital spin-alignment. While for some materials, such as Ca_2RuO_4 [8], it is reasonable to expect that our altermagnetic order will survive, beyond a certain value of J the energetic gap between the spin-aligned and anti-aligned phases (See SM [52]) should lead to its disappearance.

In this work, we have not considered the effect of spin-orbit coupling. We do not expect this to spoil our mechanism [5], but rather to enrich the phase diagram by breaking spin collinearity, thereby giving rise to non-trivial band topology [20, 62].

Acknowledgements We are grateful to C. Autieri, G. Bellomia, M. Fabrizio, R. Fernandes, M. Ferraretto, E. Linnér, J. Skolimowski, and A. Toschi for helpful discussions. This work has been supported by National Recovery and Resilience Plan (NRRP) MUR Project No. CN00000013-ICSC and PE0000023-NQSTI and by MUR via PRIN 2020 (Prot. 2020JLZ52N 002) programs, PRIN 2022 (Prot. 20228YCY7).

[1] L. Šmejkal, J. Sinova, and T. Jungwirth, Beyond conventional ferromagnetism and antiferromagnetism: A phase with nonrelativistic spin and crystal rotation symmetry, *Phys. Rev. X* **12**, 031042 (2022).
 [2] L. Šmejkal, J. Sinova, and T. Jungwirth, Emerging research landscape of altermagnetism, *Phys. Rev. X* **12**,

040501 (2022).
 [3] D.-F. Shao, S.-H. Zhang, M. Li, C. B. Eom, and E. Y. Tsymbal, Spin-neutral currents for spintronics, *Nature Communications* **12** (2021).
 [4] H. Bai, L. Han, X. Feng, Y. Zhou, R. Su, Q. Wang, L. Liao, W. Zhu, X. Chen, F. Pan, *et al.*, Observation

- of spin splitting torque in a collinear antiferromagnet ruo_2 , *Physical Review Letters* **128**, 197202 (2022).
- [5] R. González-Hernández, L. Šmejkal, K. Výborný, Y. Yahagi, J. Sinova, T. c. v. Jungwirth, and J. Železný, Efficient electrical spin splitter based on nonrelativistic collinear antiferromagnetism, *Phys. Rev. Lett.* **126**, 127701 (2021).
- [6] R. M. Sattigeri, G. Cuono, and C. Autieri, Altermagnetic surface states: towards the observation and utilization of altermagnetism in thin films, interfaces and topological materials, *Nanoscale* **15**, 16998 (2023).
- [7] A. Fakhredine, R. M. Sattigeri, G. Cuono, and C. Autieri, Interplay between altermagnetism and nonsymmorphic symmetries generating large anomalous hall conductivity by semi-dirac points induced anticrossings, *Phys. Rev. B* **108**, 115138 (2023).
- [8] G. Cuono, R. M. Sattigeri, J. Skolimowski, and C. Autieri, Orbital-selective altermagnetism and correlation-enhanced spin-splitting in strongly-correlated transition metal oxides, *Journal of Magnetism and Magnetic Materials* **586**, 171163 (2023).
- [9] M. J. Grzybowski, C. Autieri, J. Domagala, C. Krasucki, A. Kaleta, S. Kret, K. Gas, M. Sawicki, R. Božek, J. Sufczyński, and W. Pacuski, Wurtzite vs. rock-salt mnse epitaxy: electronic and altermagnetic properties, *Nanoscale* **16**, 6259 (2024).
- [10] F. Ferrari and R. Valenti, Altermagnetism on the shastry-sutherland lattice (2024), arXiv:2408.00841 [cond-mat.str-el].
- [11] R. B. Regmi, H. Bhandari, B. Thapa, Y. Hao, N. Sharma, J. McKenzie, X. Chen, A. Nayak, M. E. Gazzah, B. G. Márkus, L. Forró, X. Liu, H. Cao, J. F. Mitchell, I. I. Mazin, and N. J. Ghimire, Altermagnetism in the layered intercalated transition metal dichalcogenide comb_4ses (2024), arXiv:2408.08835 [cond-mat.str-el].
- [12] P.-H. Chang and I. I. Mazin, The mysterious magnetic ground state of $\text{ba}_1\text{4mnbi}_1$ is likely altermagnetic (2024), arXiv:2407.16019 [cond-mat.mtrl-sci].
- [13] O. E. Parfenov, D. V. Averyanov, I. S. Sokolov, A. N. Mihalyuk, O. A. Kondratev, A. N. Taldenkov, A. M. Tokmachev, and V. G. Storchak, Pushing an altermagnet to the ultimate 2d limit: Evidence of symmetry breaking in monolayers of gdalsi (2024), arXiv:2406.07172 [cond-mat.mtrl-sci].
- [14] A. Hariki, T. Okauchi, Y. Takahashi, and J. Kuneš, Determination of the néel vector in rutile altermagnets through x-ray magnetic circular dichroism: The case of mnf_2 , *Phys. Rev. B* **110**, L100402 (2024).
- [15] A. Hariki, A. Dal Din, O. J. Amin, T. Yamaguchi, A. Badura, D. Kriegner, K. W. Edmonds, R. P. Campion, P. Wadley, D. Backes, L. S. I. Veiga, S. S. Dhesi, G. Springholz, L. Šmejkal, K. Výborný, T. Jungwirth, and J. Kuneš, X-ray magnetic circular dichroism in altermagnetic α - mnTe , *Phys. Rev. Lett.* **132**, 176701 (2024).
- [16] I. Mazin, R. González-Hernández, and L. Šmejkal, Induced monolayer altermagnetism in $\text{mnp}(\text{s,se})_3$ and fese (2023), arXiv:2309.02355 [cond-mat.mes-hall].
- [17] E. F. Galindez-Ruales, L. Šmejkal, S. Das, E. Baek, C. Schmitt, F. Fuhrmann, A. Ross, R. González-Hernández, A. Rothschild, J. Sinova, C. Y. You, G. Jakob, and M. Kläui, Altermagnetism in the hopping regime (2024), arXiv:2310.16907 [cond-mat.mtrl-sci].
- [18] L. D. Re, Dirac points and topological phases in correlated altermagnets (2024), arXiv:2408.14288 [cond-mat.str-el].
- [19] Y. Yu, H.-G. Suh, M. Roig, and D. F. Agterberg, Altermagnetism from coincident van Hove singularities: application to κ - cl (2024), arXiv:2402.05180 [cond-mat.str-el].
- [20] D. S. Antonenko, R. M. Fernandes, and J. W. F. Venderbos, Mirror chern bands and weyl nodal loops in altermagnets (2024), arXiv:2402.10201 [cond-mat.mes-hall].
- [21] S. G. Jeong, I. H. Choi, S. Nair, L. Buiarelli, B. Pourbahari, J. Y. Oh, N. Bassim, A. Seo, W. S. Choi, R. M. Fernandes, T. Birol, L. Zhao, J. S. Lee, and B. Jalan, Altermagnetic polar metallic phase in ultra-thin epitaxially-strained ruo_2 films (2024), arXiv:2405.05838 [cond-mat.mtrl-sci].
- [22] Z. Lin, D. Chen, W. Lu, X. Liang, S. Feng, K. Yamagami, J. Osiecki, M. Leandersson, B. Thiagarajan, J. Liu, C. Felser, and J. Ma, Observation of giant spin splitting and d-wave spin texture in room temperature altermagnet ruo_2 (2024), arXiv:2402.04995 [cond-mat.mtrl-sci].
- [23] P. Kefler, L. Garcia-Gassull, A. Suter, T. Prokscha, Z. Salman, D. Khalyavin, P. Manuel, F. Orlandi, I. I. Mazin, R. Valenti, and S. Moser, Absence of magnetic order in ruo_2 : insights from μsr spectroscopy and neutron diffraction (2024), arXiv:2405.10820 [cond-mat.mtrl-sci].
- [24] T. Osumi, S. Souma, T. Aoyama, K. Yamauchi, A. Honma, K. Nakayama, T. Takahashi, K. Ohgushi, and T. Sato, Observation of a giant band splitting in altermagnetic mnTe , *Phys. Rev. B* **109**, 115102 (2024).
- [25] S. Reimers, L. Odenbreit, L. Šmejkal, V. N. Strocov, P. Constantinou, A. B. Hellenes, R. Jaeschke Ubiergo, W. H. Campos, V. K. Bharadwaj, A. Chakraborty, *et al.*, Direct observation of altermagnetic band splitting in crsb thin films, *Nature Communications* **15**, 2116 (2024).
- [26] V. Leeb, A. Mook, L. Šmejkal, and J. Knolle, Spontaneous formation of altermagnetism from orbital ordering, *Phys. Rev. Lett.* **132**, 236701 (2024).
- [27] Y. Nagaoka, Ferromagnetism in a narrow, almost half-filled s band, *Phys. Rev.* **147**, 392 (1966).
- [28] J. E. Hirsch, Two-dimensional hubbard model: Numerical simulation study, *Phys. Rev. B* **31**, 4403 (1985).
- [29] H. Q. Lin and J. E. Hirsch, Two-dimensional hubbard model with nearest- and next-nearest-neighbor hopping, *Phys. Rev. B* **35**, 3359 (1987).
- [30] S. Raghu, X.-L. Qi, C.-X. Liu, D. J. Scalapino, and S.-C. Zhang, Minimal two-band model of the superconducting iron oxypnictides, *Phys. Rev. B* **77**, 220503 (2008).
- [31] M. Ulmke, Ferromagnetism in the hubbard model on fcc-type lattices, *The European Physical Journal B-Condensed Matter and Complex Systems* **1**, 301 (1998).
- [32] I. Morera, M. Kanász-Nagy, T. Smolenski, L. Ciorciaro, A. m. c. Imamoğlu, and E. Demler, High-temperature ki-

- netic magnetism in triangular lattices, *Phys. Rev. Res.* **5**, L022048 (2023).
- [33] M. Lebrat, M. Xu, L. H. Kendrick, A. Kale, Y. Gang, P. Seetharaman, I. Morera, E. Khatami, E. Demler, and M. Greiner, Observation of nagaoka polarons in a fermi-hubbard quantum simulator, *Nature* **629**, 317 (2024).
- [34] M. Xu, L. H. Kendrick, A. Kale, Y. Gang, G. Ji, R. T. Scalettar, M. Lebrat, and M. Greiner, Frustration-and doping-induced magnetism in a fermi-hubbard simulator, *Nature* **620**, 971 (2023).
- [35] R. Hlubina, S. Sorella, and F. Guinea, Ferromagnetism in the two dimensional $t-t'$ hubbard model at the van hove density, *Phys. Rev. Lett.* **78**, 1343 (1997).
- [36] D. V. Chichinadze, L. Classen, and A. V. Chubukov, Valley magnetism, nematicity, and density wave orders in twisted bilayer graphene, *Phys. Rev. B* **102**, 125120 (2020).
- [37] L. Classen, A. V. Chubukov, C. Honerkamp, and M. M. Scherer, Competing orders at higher-order van hove points, *Phys. Rev. B* **102**, 125141 (2020).
- [38] N. Lanatà, Operatorial formulation of the ghost rotationally invariant slave-boson theory, *Phys. Rev. B* **105**, 045111 (2022).
- [39] F. Lechermann, A. Georges, G. Kotliar, and O. Parcollet, Rotationally invariant slave-boson formalism and momentum dependence of the quasiparticle weight, *Phys. Rev. B* **76**, 155102 (2007).
- [40] A. Isidori and M. Capone, Rotationally invariant slave bosons for strongly correlated superconductors, *Phys. Rev. B* **80**, 115120 (2009).
- [41] N. Lanatà, T.-H. Lee, Y.-X. Yao, and V. Dobrosavljević, Emergent bloch excitations in mott matter, *Phys. Rev. B* **96**, 195126 (2017).
- [42] D. Guerci, M. Capone, and M. Fabrizio, Exciton mott transition revisited, *Phys. Rev. Mater.* **3**, 054605 (2019).
- [43] M. S. Frank, T.-H. Lee, G. Bhattacharyya, P. K. H. Tsang, V. L. Quito, V. Dobrosavljević, O. Christiansen, and N. Lanatà, Quantum embedding description of the anderson lattice model with the ghost gutzwiller approximation, *Phys. Rev. B* **104**, L081103 (2021).
- [44] C. Mejuto-Zaera and M. Fabrizio, Efficient computational screening of strongly correlated materials: Multiorbital phenomenology within the ghost gutzwiller approximation, *Phys. Rev. B* **107**, 235150 (2023).
- [45] D. Guerci, M. Capone, and N. Lanatà, Time-dependent ghost gutzwiller nonequilibrium dynamics, *Phys. Rev. Res.* **5**, L032023 (2023).
- [46] T.-H. Lee, C. Melnick, R. Adler, N. Lanatà, and G. Kotliar, Accuracy of ghost-rotationally-invariant slave-boson theory for multiorbital hubbard models and realistic materials, *Phys. Rev. B* **108**, 245147 (2023).
- [47] T.-H. Lee, N. Lanatà, and G. Kotliar, Accuracy of ghost rotationally invariant slave-boson and dynamical mean field theory as a function of the impurity-model bath size, *Phys. Rev. B* **107**, L121104 (2023).
- [48] C. Mejuto-Zaera, Quantum embedding for molecules using auxiliary particles – the ghost gutzwiller ansatz, *Faraday Discuss.* , (2024).
- [49] T.-H. Lee, C. Melnick, R. Adler, X. Sun, Y. Yao, N. Lanatà, and G. Kotliar, Charge self-consistent density functional theory plus ghost rotationally-invariant slave-boson theory for correlated materials, arXiv:2406.04636 (2024).
- [50] M. Fabrizio, Gutzwiller description of non-magnetic mott insulators: Dimer lattice model, *Phys. Rev. B* **76**, 165110 (2007).
- [51] N. Lanatà, Y. Yao, C.-Z. Wang, K.-M. Ho, and G. Kotliar, Phase diagram and electronic structure of praseodymium and plutonium, *Phys. Rev. X* **5**, 011008 (2015).
- [52] See Supplemental Material at XXX for a summary of the computation of the conductivity in linear response, a complement to the discussion on the tuneability of the spin currents in the strong coupling altermagnetic phase, and a brief recap of the main equations in the gRISB formalism.
- [53] B. S. Shastry and B. Sutherland, Twisted boundary conditions and effective mass in heisenberg-ising and hubbard rings, *Phys. Rev. Lett.* **65**, 243 (1990).
- [54] D. J. Scalapino, S. R. White, and S. C. Zhang, Superfluid density and the drude weight of the hubbard model, *Phys. Rev. Lett.* **68**, 2830 (1992).
- [55] Y. Tang, L. Li, T. Li, Y. Xu, S. Liu, K. Barmak, K. Watanabe, T. Taniguchi, A. H. Macdonald, J. Shan, and K. F. Mak, Simulation of hubbard model physics in wse₂/ws₂ moiré superlattices, *Nature* **579**, 353 (2020).
- [56] K. Lee, P. Sharma, O. Vafek, and H. J. Changlani, Triangular lattice hubbard model physics at intermediate temperatures, *Phys. Rev. B* **107**, 235105 (2023).
- [57] P. Potasz, N. Morales-Durán, N. C. Hu, and A. H. MacDonald, Itinerant ferromagnetism in transition metal dichalcogenide moiré superlattices, *Phys. Rev. B* **109**, 045144 (2024).
- [58] S. Sheoran and S. Bhattacharya, Nonrelativistic spin splittings and altermagnetism in twisted bilayers of centrosymmetric antiferromagnets, *Phys. Rev. Mater.* **8**, L051401 (2024).
- [59] S.-D. Guo, Y. Liu, and C.-C. Liu, Valley polarization in twisted altermagnetism (2024), arXiv:2406.13950 [cond-mat.mtrl-sci].
- [60] M. Capone, M. Fabrizio, C. Castellani, and E. Tosatti, Strongly correlated superconductivity, *Science* **296**, 2364 (2002).
- [61] M. Capone, M. Fabrizio, C. Castellani, and E. Tosatti, Colloquium: Modeling the unconventional superconducting properties of expanded A_3C_{60} fullerides, *Rev. Mod. Phys.* **81**, 943 (2009).
- [62] L. Šmejkal, R. González-Hernández, T. Jungwirth, and J. Sinova, Crystal time-reversal symmetry breaking and spontaneous hall effect in collinear antiferromagnets, *Science Advances* **6**, eaaz8809 (2020), <https://www.science.org/doi/pdf/10.1126/sciadv.aaz8809>.

Appendix A: Conductivity and Drude weight

In presence of a vector potential A that is approximately constant at the lattice scale, the Peierls substitution consists in replacing the hopping integrals as follows:

$$t_{ij} \rightarrow t_{ij} \exp \left\{ -i \frac{e}{\hbar} \int_{\mathbf{R}_i}^{\mathbf{R}_j} \mathbf{A}(\mathbf{r}, t) \cdot d\mathbf{r} \right\} \quad (\text{A1})$$

We consider a vector potential in the [110] direction, i.e., $(\mathbf{A})_x = (\mathbf{A})_y$ and $(\mathbf{A})_z = 0$. Expanding the kinetic terms of the full energy for small uniform vector potentials we find:

$$\begin{aligned} \hat{K} &= \sum_{ij, \alpha\beta} t_{ij}^{\alpha\beta} c_{\mathbf{R}_i\alpha}^\dagger c_{\mathbf{R}_j\beta} \{ 1 + i \frac{e}{\hbar} \mathbf{A}(t) \cdot (\mathbf{R}_i - \mathbf{R}_j) \\ &\quad - \frac{1}{2} (\frac{e}{\hbar})^2 [\mathbf{A}(t) \cdot (\mathbf{R}_i - \mathbf{R}_j)]^2 + \mathcal{O}(\mathbf{A}^3) \} \end{aligned} \quad (\text{A2})$$

with $\alpha, \beta = (\sigma, m)$ spin-orbital indexes. Replacing $\mathbf{R}_i = \mathbf{R}$ and $\mathbf{R}_i - \mathbf{R}_j = \mathbf{d}$ The total current in the $a = x, y$ direction is given by:

$$\hat{J}_a = \frac{\delta \hat{K}}{\delta A_a} = \sum_{\mathbf{R}\mathbf{d}} \sum_{\alpha\beta} t_{\mathbf{R}, \mathbf{R}+\mathbf{d}}^{\alpha\beta} c_{\mathbf{R}\alpha}^\dagger c_{\mathbf{R}+\mathbf{d}\beta} \left[-i \frac{e}{\hbar} d_a + \left(\frac{e}{\hbar} \right)^2 d_a \mathbf{d} \cdot \mathbf{A}(t) \right] \quad (\text{A3})$$

$$= e [\hat{J}_a^P + \hat{J}_a^D] \quad (\text{A4})$$

with a paramagnetic contribution (\hat{J}_a^P) independent from \mathbf{A} and a diamagnetic contribution (\hat{J}_a^D) that is \mathbf{A} dependent. In units for which $c = \hbar = 1$, one defines the conductivity σ in linear response as:

$$j_a(\omega) = \sigma_{ab}(\omega) \epsilon_b(\omega) \quad (\text{A5})$$

where $j_a = \langle \hat{J}_a \rangle$, and

$$\mathbf{A}(\omega) = \frac{\epsilon(\omega)}{i(\omega + i0^+)}. \quad (\text{A6})$$

From this, it follows that one can rewrite j_a as

$$j_a(\omega) \frac{1}{i(\omega + i0^+)} = \sigma_{ab}(\omega) A_b(\omega). \quad (\text{A7})$$

Therefore the conductivity for spin s can be computed from the contribution to first order in \mathbf{A} to the total current as:

$$\sigma_{ab}^s(\omega) = -e^2 \frac{\langle \frac{1}{V_{BZ}} \sum_{\mathbf{k}} \partial_{k_a} \partial_{k_b} H^s(\mathbf{k}) \rangle - \Lambda_{ab}^s(\omega)}{i(\omega + i0^+)} \quad (\text{A8})$$

with $\langle \frac{1}{N_k} \sum_{\mathbf{k}} \partial_{k_a} \partial_{k_b} H^s(\mathbf{k}) \rangle$ the expectation value of the second derivative of the kinetic Hamiltonian for spin s in the a and b directions in reciprocal space and Λ_{ab}^s the uniform paramagnetic current (\hat{J}^P) susceptibility for spin s that we compute as the solely elementary bubble, that is:

$$\begin{aligned} \Lambda_{ab}^s(\omega) &= \frac{1}{V_{BZ}} \sum_{\mathbf{k}} \int_{\omega_1} \int_{\omega_2} \frac{1}{\pi^2} \text{Tr} \left[\text{Im} \left\{ \hat{G}^{s}(\mathbf{k}, \omega_1) \right\} \hat{V}_a \right. \\ &\quad \left. \text{Im} \left\{ (\hat{G}^s)^T(\mathbf{k}, \omega_2) \right\} \hat{V}_b \right] \frac{f_{FD}(\omega_1) - f_{FD}(\omega_2)}{\omega_1 - \omega_2 + \omega + i0^+} \end{aligned} \quad (\text{A9})$$

with \hat{G} the Green's function in the spinorial representation for the orbitals and \hat{V}_a is the current vertex along direction a . The Drude weight is the residue of the pole at $\omega = 0$ of the conductivity:

$$D_{ab}^s = -e^2 \left[\left\langle \frac{1}{V_{BZ}} \sum_{\mathbf{k}} \partial_{k_a} \partial_{k_b} H^s(\mathbf{k}) \right\rangle - \text{Re} \{ \Lambda_{ab}^s(\omega = 0) \} \right] \quad (\text{A10})$$

Appendix B: Current inversion

In Figure 3 panel (b) we show that the spin current present an inversion along a line in the $U - \delta$ space. This inversion can be understood by looking at the contributions coming purely from orbital x and y to the diamagnetic component of the Drude weight, i.e., the Hessian of the non-interacting Hamiltonian in k -space. Namely we can compare the \mathbf{k} -space resolved contributions to the Drude weight along x direction of the two orbitals for each spin s and orbital α , that are:

$$[\tilde{j}_\alpha^s(\mathbf{k})]_x = (-1)^s \langle \partial_{k_x} \partial_{k_x} (H_{\mathbf{k}}^s)_{\alpha\alpha} \rangle \quad (\text{B1})$$

We show such contributions in Fig. 4. From left to right, increasing the interaction U we see that for orbital X it is the up current that is strengthened ($[\tilde{j}_x^\uparrow(\mathbf{k})]_x > [\tilde{j}_x^\downarrow(\mathbf{k})]_x$) while for orbital Y it is the down current ($[\tilde{j}_y^\downarrow(\mathbf{k})]_x > [\tilde{j}_y^\uparrow(\mathbf{k})]_x$). This means the two orbitals have spin-polarized currents, as to be expected since they are ferromagnetically ordered. This ordering is enhanced by increasing U . Moreover, we see that the biggest contribution to the spin current comes from the pockets found around the X point in the Brillouin zone. If we look at the spin resolved, orbital-diagonal contributions to the diamagnetic Drude weight we can see that a crossing happens at a finite value of the interaction (See Fig. 5), or similarly a finite value of the doping due to a different slope of as a function of U for the currents associated to the two spin components.

The Drude weight for small U/t is dominated by spin- \uparrow electrons, belonging mostly to orbital X (See Figure 4) while increasing U and crossing the spin-current inversion line the majority carriers become spin- \downarrow electrons belonging to orbital Y. This phenomenon can be understood in terms of an effective Drude model for the pockets at the point X in the Brillouin zone. For a free electron gas the Drude weight is $D = \frac{e^2 \pi n}{m}$ with n the number and m the mass of the electrons. In our case the spin- \uparrow and spin- \downarrow electrons have different masses due to the different orbital nature. Moreover their chemical potentials are also different due to the magnetic ordering. The number of spin- s electrons for the pocket around the X point is proportional to the integral of the paraboloid centered in X. For a paraboloid of height h and radius r the volume is given by $(\pi/2)r^2 h$. In our case the height is given by the electrochemical potential μ_s . The radius instead can be obtained from $(\mathbf{k} - \mathbf{k}_X)^2 / (2m_s) = -\mu_s$ where $r^2 = (\mathbf{k} - \mathbf{k}_X)^2 = -2m_s \mu_s$. Note that in the parabolic approximation $(\mathbf{k} - \mathbf{k}_X)^2$ is constant therefore $\mu_s \propto -1/m_s$. From this approximation we can say that the spin resolved Drude weight must be $D_s \propto -\mu_s/m_s$. Doping the altermagnet in a rigid band approximation can be seen has a rigid shift of μ_s for both spin types. Doping with holes is a positive shift in μ_s therefore for a fixed change in doping the Drude weight for the two spins is increased proportionally to their inverse mass. The effective mass of the spin- \downarrow electrons at the Fermi level is smaller and their contribution to the Drude weight decreases less than the spin- \uparrow with a larger mass at the Fermi level. The two Drude weights as a function of doping therefore have different slopes and meet at a finite value of the doping. The effect of the interaction U instead is to increase the magnetic gap therefore increasing the splitting between μ_\uparrow and μ_\downarrow . This is easily obtained at mean-field level, but it is expected to be a general effect. Similarly, in a theory with fixed masses m_s this will lead to an increase of μ_\downarrow with respect to μ_\uparrow .

Appendix C: gRISB equations

In this appendix we succinctly summarize the main ingredients and the algorithmic structure of the gRISB method with mean-field treatment of the bosons. As noted in the main body of the paper, this is equivalent to the ghost Gutzwiller approach. For a more detailed discussion of the origin and heuristic meaning of the equations, as well as implementational details, we refer to previous work in the field [41, 44, 48] and references therein.

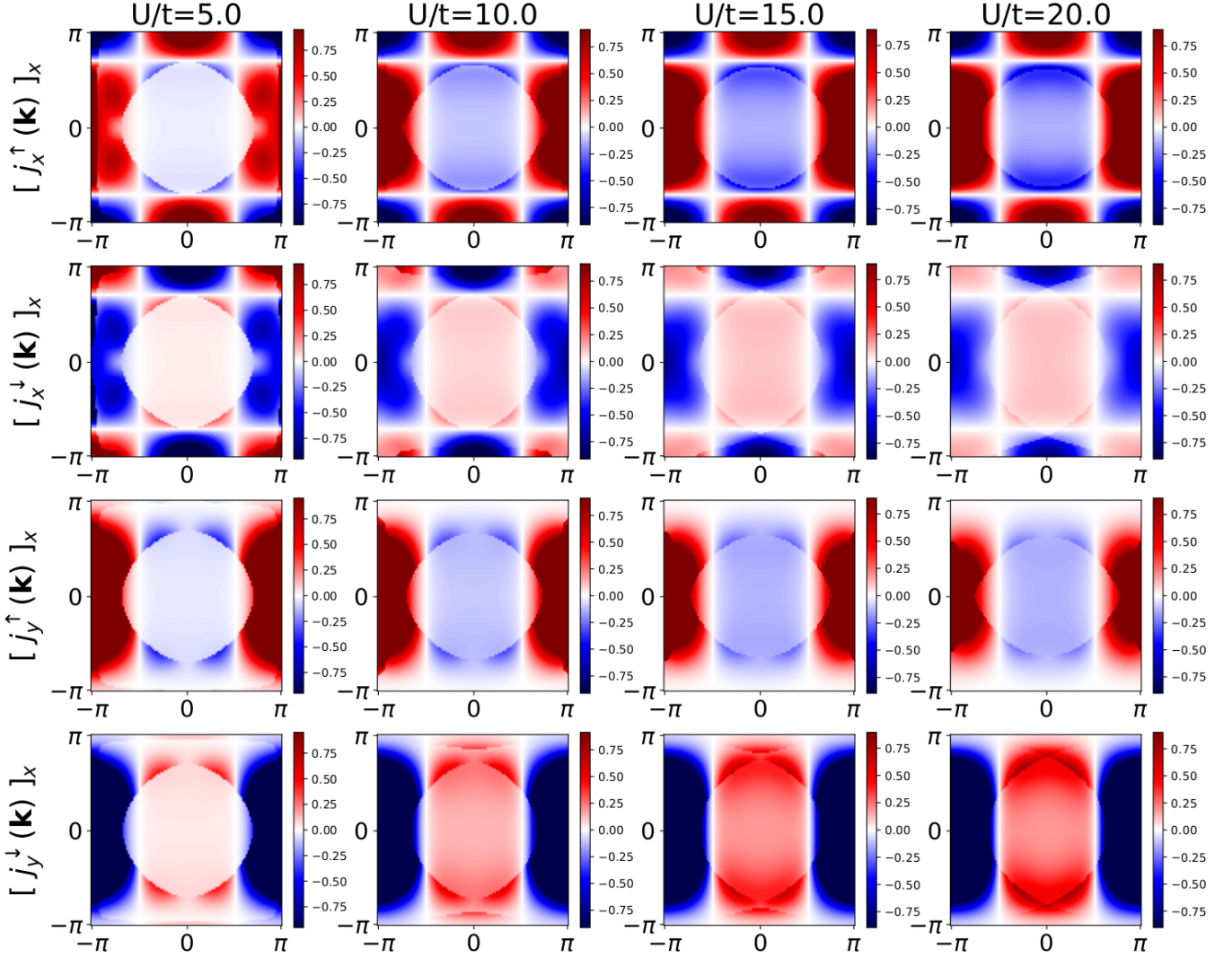


Figure 4: Momentum resolved contributions to the diamagnetic Drude weight, orbital and spin diagonal for doping $\delta = -0.13$. From left to right the interactions $U/t = 5, 10, 15, 20$. From top to bottom the spin- \uparrow orbital X, spin- \downarrow orbital X, spin- \uparrow orbital Y and spin- \downarrow orbital Y.

For simplicity, we shall assume that we are interested in a lattice Hamiltonian with space translation invariance of the form

$$H_{phys} = \sum_I H_I^{loc} + H_{latt}, \quad (C1)$$

where capital indices I run over lattice sites, H_I^{loc} represents the local, possibly interacting, site Hamiltonian

$$H_I^{loc} = \sum_{\alpha\beta} t_{\alpha\beta}^I c_{I\alpha}^\dagger c_{I\beta} + \sum_{\alpha\beta\gamma\delta} U_{\alpha\beta;\gamma\delta} c_{I\alpha}^\dagger c_{I\gamma}^\dagger c_{I\delta} c_{I\beta}, \quad (C2)$$

and H_{latt} is the non-interacting lattice Hamiltonian, including the inter-site hopping terms

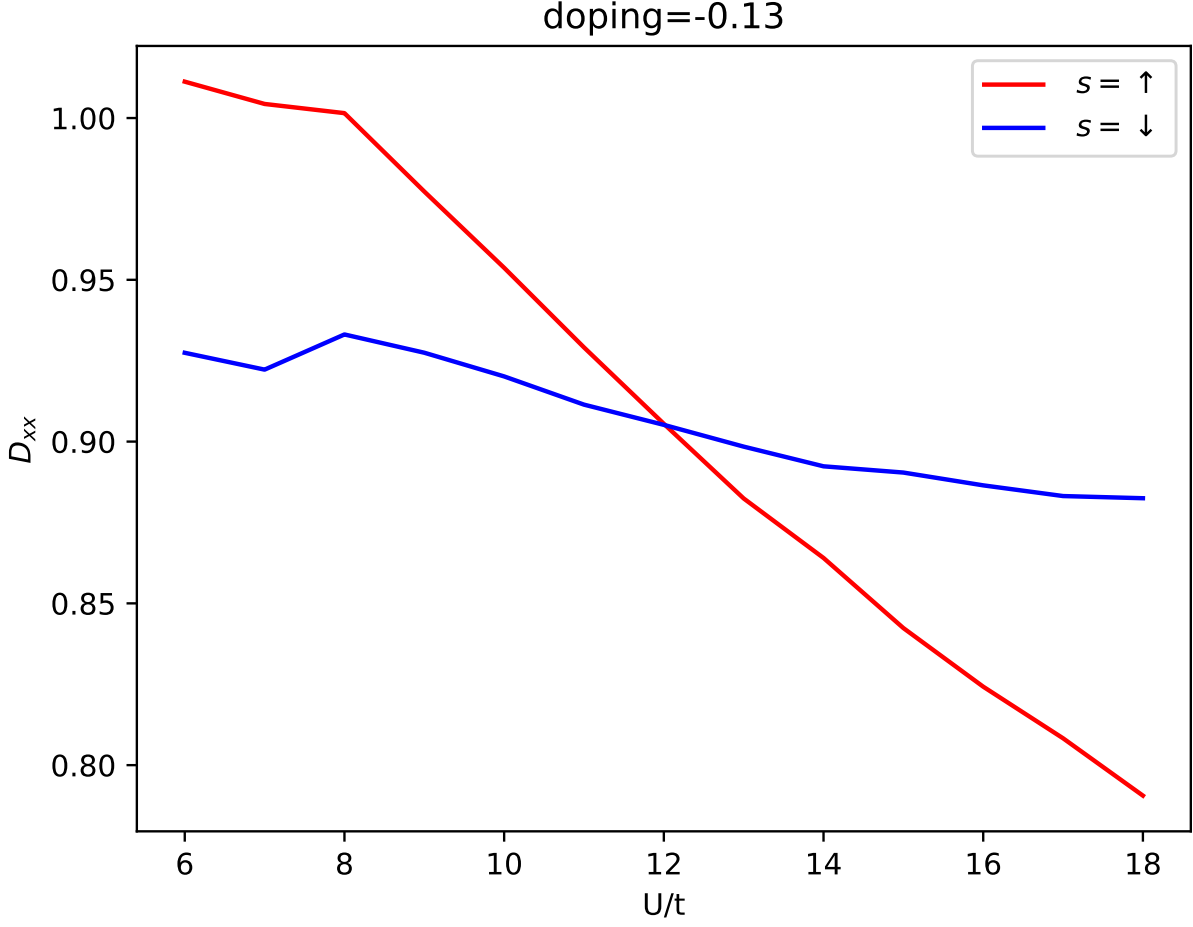


Figure 5: Orbital-diagonal contributions to the diamagnetic Drude weight for doping $\delta = -0.13$

$$H_{latt} = \sum_{I \neq J} \sum_{\alpha\beta} t_{\alpha\beta}^{IJ} c_{I\alpha}^\dagger c_{J\beta} = \sum_{\mathbf{k}} \sum_{\alpha\beta} \epsilon_{\alpha\beta}(\mathbf{k}) c_{\mathbf{k}\alpha}^\dagger c_{\mathbf{k}\beta}. \quad (\text{C3})$$

The orbitals of the physical Hamiltonian are indicated with Greek indices $\alpha, \beta, \gamma, \delta$, and may include the spin index. In the last equality of Eq. (C3) we have used the space translational invariance to write the lattice Hamiltonian in momentum space, with the band structure dispersion $\epsilon_{\alpha\beta}(\mathbf{k})$. Within its embedding formulation, gRISB maps H_{phys} into a quasiparticle Hamiltonian H_{qp} . This is an effective, non-interacting Hamiltonian, in which correlation effects are represented in terms of band structure renormalizations R and potentially local one-body potentials λ . This leads to

$$H_{qp} = \sum_{\mathbf{k}} \sum_{ab} \left[\sum_{\alpha\beta} R_{a\alpha}^\dagger \epsilon_{\alpha\beta}(\mathbf{k}) R_{\beta b} - \lambda_{ab} \right] d_{\mathbf{k}a}^\dagger d_{\mathbf{k}b}, \quad (\text{C4})$$

where we use Latin indices to distinguish quasiparticle orbitals from physical ones, besides denoting the creation operators with the letter d instead of c . Additionally, we may choose to define H_{qp} over an enlarged Hilbert space by

including the so-called ghost orbitals to improve the description of strong correlation [41, 44].

The parameters R and λ in H_{qp} are self-consistently determined with the solution of an impurity model H_{imp} , which brings in information about the local interactions in the system. This impurity model contains the physical orbitals of a single site in H_{phys} , dressed by a non-interacting quasiparticle bath, such that

$$H_{imp} = H_0^{loc} + \sum_{\alpha a} (V_{a\alpha} d_a^\dagger c_\alpha + \text{h.c.}) - \sum_{ab} \lambda_{ab}^c d_b d_a^\dagger. \quad (\text{C5})$$

Here, H_0^{loc} denotes the local Hamiltonian contribution for some arbitrary site in the lattice (as all are equal by translational invariance). The bath parameters V (hybridizations) and λ^c (local potential) are also determined self-consistently, by imposing that the ground state local one body reduced density matrices of H_{qp} and H_{imp} match

$$\langle d_b d_a^\dagger \rangle_{imp} \stackrel{!}{=} \langle d_{0a}^\dagger d_{0b} \rangle_{qp} \equiv \Delta_{ab}^{qp}. \quad (\text{C6})$$

Again, d_{0a}^\dagger denotes orbital a at an arbitrary lattice site. This self-consistency can be achieved iteratively, starting from some guess R and λ parameters, as follows:

1. The current R and λ define a H_{qp} according to Eq. (C4). From this, compute the ground state energy and local 1RDM $\Delta_{ab}^{qp} = \langle d_{0a}^\dagger d_{0b} \rangle_{qp}$.
2. Evaluate the impurity model parameters V and λ^c . These can be computed from the H_{qp} ground state. The hybridization V follows

$$V = \frac{1}{V_{BZ}} \sqrt{\Delta^{qp}(\mathbb{I} - \Delta^{qp})}^{-1} \cdot \sum_{\mathbf{k}} \Delta_{\mathbf{k}}^t \cdot R^\dagger \cdot \epsilon(\mathbf{k}), \quad (\text{C7})$$

where V_{BZ} is the Brillouin zone volume, and $\Delta_{\mathbf{k}} = \langle d_{\mathbf{k}a}^\dagger d_{\mathbf{k}b} \rangle_{qp}$. The local potential λ^c follows

$$\lambda_{ab}^c = -\lambda_{ab} + \frac{\partial}{\partial \Delta_{ab}^{qp}} \text{Tr} \left[R \cdot \sqrt{\Delta^{qp}(\mathbb{I} - \Delta^{qp})} \cdot V \right] + \text{h.c.}, \quad (\text{C8})$$

where the derivative acts only on the term on the square root.

3. Solve the impurity model in Eq. C5 with the previously determined V and λ^c , and evaluate the impurity model ground state density matrix elements $\langle c_\alpha^\dagger d_a \rangle_{imp}$ and $\langle d_a^\dagger d_b \rangle_{imp}$.
4. From the solution of the impurity model, the next guess for R and λ can be determined. For this, we need to first determine the new quasiparticle density matrix as

$$\Delta_{ab}^{qp} = \mathbb{I} - \langle d_a^\dagger d_b \rangle_{imp}. \quad (\text{C9})$$

From this, the new R parameter can be obtained from

$$\sum_a R_{\alpha a} \left[\sqrt{\Delta^{qp}(\mathbb{I} - \Delta^{qp})} \right]_{ab} = \langle c_{I\alpha}^\dagger d_b \rangle_{imp}. \quad (\text{C10})$$

Finally, to evaluate a new λ there are two possible strategies: determining it through a fitting problem, to enforce that the local one-body density matrix of the new H_{qp} matches the Δ^{qp} obtained in Eq. (C9) (cf. Ref. [44]), or alternatively to invert Eq. (C8) solving it for λ instead of λ_c (cf. Ref. [48]). At self-consistency, both approaches lead to the same solution.

5. If the new R , λ match the ones from the previous iteration to some tolerance, the algorithm can be stopped at the stage. Otherwise, return to step 1.

It is worth noting that, within the infinite dimensional limit, this self-consistency procedure is equivalent to variationally optimizing a Gutzwiller-like wave function Ansatz for the lattice [50, 51]. Upon convergence, local observables can be directly obtained from the impurity model, whereas non-local observables can be extracted from the quasiparticle Hamiltonian. In particular, the Green's function can be estimated by projecting the quasiparticle Green's function into the physical orbitals as

$$G_{\alpha\beta}(\omega, \mathbf{k}) = \sum_{ab} R_{\alpha a} \left[\frac{1}{(\omega + i0^+) \mathbb{I} - H_{qp}(\mathbf{k})} \right]_{ab} R_{b\beta}^\dagger. \quad (\text{C11})$$

Essentially, this allows to map the spectrum of the correlated model into a band structure theory in a larger Hilbert space. From this Green's function we extract the band structures shown in the main paper. The ground state energy per site of the model, which we use to compare phase stability invoking the underlying variability of the method, can be reconstructed from the ground state energy of the impurity model and the density matrix of the quasiparticle Hamiltonian as

$$E_0^G/N = E_{imp} + \frac{1}{V_{BZ}} \sum_{\mathbf{k}} \sum_{ab} \left(\sum_{\alpha\beta} R_{\alpha a}^\dagger \epsilon_{\alpha\beta}(\mathbf{k}) R_{\beta b} \right) \Delta_{ab}^{qp}(\mathbf{k}). \quad (\text{C12})$$

Appendix D: Energetic stability of altermagnetism over ferromagnetism

We present a simple mean-field argument that shows that the local altermagnetic phase we present is energetically more stable than a ferromagnetic state, where the spin on the two orbitals are aligned.

Consider the Hamiltonian in Eq. (1), where the t_4 NNN inter-orbital hopping is set to zero. This correspond to two decoupled square-lattice Hubbard models. In the vicinity of the van Hove singularity the single Hubbard models will order ferromagnetically. Consider ordering in the σ_z direction, at mean-field level the models will now have the following Hamiltonian:

$$\hat{H}_{2FM} = \sum_{\mathbf{k}, s} \begin{pmatrix} c_{\mathbf{k}xs}^\dagger & c_{\mathbf{k}ys}^\dagger \end{pmatrix} \begin{pmatrix} \epsilon_x(\mathbf{k}) + (-1)^s m_x & 0 \\ 0 & \epsilon_y(\mathbf{k}) + (-1)^s m_y \end{pmatrix} \begin{pmatrix} c_{\mathbf{k}x} \\ c_{\mathbf{k}y} \end{pmatrix} \quad (\text{D1})$$

with $m_x, m_y = \pm m$. Consider the ferromagnetic case, namely $m_x = m_y = m$. We call $\epsilon^+ = \frac{\epsilon_x(\mathbf{k}) + \epsilon_y(\mathbf{k})}{2}$, $\epsilon^- = \frac{\epsilon_x(\mathbf{k}) - \epsilon_y(\mathbf{k})}{2}$ and $h(\mathbf{k})$ the inter-orbital hopping in reciprocal space. Adding back the inter-orbital hopping would result for each \mathbf{k} in the following 4 eigenvalues:

$$\begin{aligned} \varepsilon_1^{FM} &= \epsilon^+ + m + \sqrt{(\epsilon^-)^2 + h^2} \\ \varepsilon_2^{FM} &= \epsilon^+ + m - \sqrt{(\epsilon^-)^2 + h^2} \\ \varepsilon_3^{FM} &= \epsilon^+ - m + \sqrt{(\epsilon^-)^2 + h^2} \\ \varepsilon_4^{FM} &= \epsilon^+ - m - \sqrt{(\epsilon^-)^2 + h^2} \end{aligned}$$

The two lowest ones will be either $\varepsilon_2^{FM}, \varepsilon_4^{FM}$ or $\varepsilon_3^{FM}, \varepsilon_4^{FM}$.

For the altermagnetic case instead the magnetisation are opposite ($m_x = -m_y = m$) and the eigenvalues would be:

$$\begin{aligned} \varepsilon_1^{ALM} &= \epsilon^+ + \sqrt{(\epsilon^- + m)^2 + h^2} \\ \varepsilon_2^{ALM} &= \epsilon^+ + \sqrt{(\epsilon^- - m)^2 + h^2} \\ \varepsilon_3^{ALM} &= \epsilon^+ - \sqrt{(\epsilon^- + m)^2 + h^2} \\ \varepsilon_4^{ALM} &= \epsilon^+ - \sqrt{(\epsilon^- - m)^2 + h^2} \end{aligned}$$

with $\varepsilon_3^{ALM}, \varepsilon_4^{ALM}$ always being the smallest ones. It is easy to verify that the sum of eigenvalues coming from the latter ordering are always smaller than the ferromagnetic ones, therefore the uniform altermagnetic ordering is favored over the ferromagnetic phase. We have to consider two cases.

a. First case: $m > \sqrt{(\varepsilon^-)^2 + h^2}$

In this case we need to prove that

$$\sqrt{(\varepsilon^- - m)^2 + h^2} + \sqrt{(\varepsilon^- + m)^2 + h^2} > 2m \quad (\text{D2})$$

We first rewrite this as:

$$m \left[\sqrt{1 + \left(\frac{h}{m}\right)^2 + \left(\frac{\varepsilon^-}{m}\right)^2} + 2\frac{\varepsilon^-}{m} + \sqrt{1 + \left(\frac{h}{m}\right)^2 + \left(\frac{\varepsilon^-}{m}\right)^2} - 2\frac{\varepsilon^-}{m} \right] > 2m \quad (\text{D3})$$

Introducing $x = \frac{\varepsilon^-}{m}$ and $y = \frac{h}{m}$ it is easy to prove that

$$\sqrt{1 + y^2 + x^2 + 2x} + \sqrt{1 + y^2 + x^2 - 2x} - 2 > 0 \quad (\text{D4})$$

The left-hand side is zero only when $y = 0$, that correspond to $h = 0$, a sub-set of zero measure in the Brillouin Zone.

b. Second case: $m < \sqrt{(\varepsilon^-)^2 + h^2}$

In this case we need to prove that

$$\sqrt{(\varepsilon^- - m)^2 + h^2} + \sqrt{(\varepsilon^- + m)^2 + h^2} > 2\sqrt{h^2 + \varepsilon^2} \quad (\text{D5})$$

We rewrite the equation as

$$\sqrt{(\varepsilon^-)^2 + h^2} \left[\sqrt{1 + \frac{m^2}{h^2 + (\varepsilon^-)^2} + \frac{2m\varepsilon^-}{h^2 + (\varepsilon^-)^2}} + \sqrt{1 + \frac{m^2}{h^2 + (\varepsilon^-)^2} - \frac{2m\varepsilon^-}{h^2 + (\varepsilon^-)^2}} \right] > 2\sqrt{h^2 + \varepsilon^2} \quad (\text{D6})$$

We then call $y = \frac{m}{\sqrt{h^2 + (\varepsilon^-)^2}}$ and $x = \frac{2\varepsilon^- m}{h^2 + (\varepsilon^-)^2}$.

Clearly when $m > 2\varepsilon$ both terms in the square parenthesis on the left are greater than 1 and the condition is easily realised. If $m = 2\varepsilon$ the left- and right-sides of the equation are equal but this correspond again to a zero measure set of the BZ.

When $m < 2\varepsilon$ instead we can square Eq. (D6) and obtain:

$$2\frac{m^2}{h^2 + (\varepsilon^-)^2} + 2\sqrt{\left(1 + \frac{m^2}{h^2 + (\varepsilon^-)^2}\right)^2 - \left(\frac{2\varepsilon^- m}{h^2 + (\varepsilon^-)^2}\right)^2} > 0, \quad (\text{D7})$$

which is always realised. Therefore the altermagnetic phase is always energetically favorable with respect to the ferromagnetic one due to the presence of inter-orbital hoppings.

Appendix E: Existence of Dirac points

The existence of Dirac points is linked to the magnitude of the magnetic gap. Consider in particular a intra-orbital magnetic gap Δ_{mag} that is opposite for the two orbitals as in our altermagnetic state. The low energy Hamiltonian in reciprocal space will read:

$$\hat{H}_{\mathbf{k},s} = \begin{pmatrix} c_{\mathbf{k}xs}^\dagger & c_{\mathbf{k}ys}^\dagger \end{pmatrix} \begin{pmatrix} \varepsilon_x(\mathbf{k}) + (-1)^s \Delta_{mag} & \varepsilon_{xy}(\mathbf{k}) \\ \varepsilon_{xy}(\mathbf{k}) & \varepsilon_y(\mathbf{k}) - (-1)^s \Delta_{mag} \end{pmatrix} \begin{pmatrix} c_{\mathbf{k}xs} \\ c_{\mathbf{k}ys} \end{pmatrix} \quad (\text{E1})$$

that has eigenvalues:

$$\varepsilon_{\pm}(\mathbf{k}) = \varepsilon^+(\mathbf{k}) \pm \sqrt{[\varepsilon^-(\mathbf{k}) + \Delta_{mag}]^2 + [\varepsilon_{xy}(\mathbf{k})]^2} \quad (\text{E2})$$

with

$$\epsilon^\pm(\mathbf{k}) = \frac{\epsilon_x(\mathbf{k}) \pm \epsilon_y(\mathbf{k})}{2} \quad (\text{E3})$$

Dirac points appear for k-points that cancel the square root terms in the eigenvalues, that is

$$\epsilon^-(\mathbf{k}) + \Delta_{mag} = 0 \quad (\text{E4})$$

$$\epsilon_{xy}(\mathbf{k}) = 0 \quad (\text{E5})$$

The former cannot be verified for

$$\frac{\Delta_{mag}}{|t_1 - t_2|} > 1 \quad (\text{E6})$$
